Radial fast-neutron fluence gradients during rotating ^{40}Ar/^{39}Ar sample irradiation recorded with metallic fluence monitors and geological age standards

Daniel Rutte[1], Jörg A. Pfänder[1], Michal Koleška[2], Raymond Jonckheere[1,3], and Sepp Unterricker[4,5]

[1]Institut für Geologie, TU Bergakademie Freiberg, Freiberg, Germany, [2]Research Centre Řež, Řež, Czech Republic, [3]Geologie en Bodemkunde, Universiteit Gent, Gent, Belgium, [4]Institut für Angewandte Physik, TU Bergakademie Freiberg, Freiberg, Germany, [5]Deceased 31 May 2014

Abstract Characterizing the neutron-irradiation parameter J is one of the major uncertainties in ^{40}Ar/^{39}Ar dating. The associated uncertainty of the individual J-value for a sample of unknown age depends on the accuracy of the age of the geological standards, the fast-neutron fluence distribution in the reactor, and the distances between standards and samples during irradiation. While it is generally assumed that rotating irradiation evens out radial neutron fluence gradients, we observed axial and radial variations of the J-values in sample irradiations in the rotating channels of two reactors. To quantify them, we included three-dimensionally distributed metallic fast (Ni) and thermal- (Co) neutron fluence monitors in three irradiations and geological age standards in three more. Two irradiations were carried out under Cd shielding in the FRG1 reactor in Geesthacht, Germany, and four without Cd shielding in the LVR-15 reactor in Řež, Czech Republic. The ^{58}Ni(n$_f$,p)^{58}Co activation reaction and γ-spectrometry of the 811 keV peak associated with the subsequent decay of ^{58}Co to ^{58}Fe allow one to calculate the fast-neutron fluence. The fast-neutron fluences at known positions in the irradiation container correlate with the J-values determined by mass-spectrometric ^{40}Ar/^{39}Ar measurements of the geological age standards. Radial neutron fluence gradients are up to 1.8 %/cm in FRG1 and up to 2.2 %/cm in LVR-15; the corresponding axial gradients are up to 5.9 and 2.1 %/cm. We conclude that sample rotation might not always suffice to meet the needs of high-precision dating and gradient monitoring can be crucial.

1. Introduction

The ^{40}Ar/^{39}Ar dating method has several advantages over the traditional ^{40}K/^{40}Ar method in geosciences. The parent and daughter isotopes are measured through the same element on the same aliquot in one mass spectrometer, increasing the analytical accuracy and allowing spot measurements using laser ablation. The thermal histories of the samples can be inferred from step-heating experiments that also provide internal consistency checks. The disadvantage is the need for fast-neutron irradiation to activate the ^{39}K(n$_f$,p)^{39}Ar reaction, after which ^{39}Ar serves as a proxy for the ^{40}K-content. Co-irradiated geological age standards are used to monitor the reaction rate. Several studies addressed the absolute and cross calibration of geological age standards and invested considerable effort in improving the precision of their reference ages [e.g., *Roddick*, 1983; *Baksi et al.*, 1995; *Renne et al.*, 1998; *Kuiper et al.*, 2008; *Renne et al.*, 2010, 2011; *Boehnke and Harrison*, 2014]. The irradiation also has undesirable nuclear effects. Recoil losses of ^{39}Ar after proton emission require additional analytical effort or correction, in particular for fine-grained samples [e.g., *Smith et al.*, 1993; *Onstott et al.*, 1995]. The production of interfering Ar isotopes from K, Ca, and Cl has to be minimized and corrected for [e.g., *Turner*, 1995; *Renne et al.*, 2005]. Recent improvements in the precision of the ^{40}Ar/^{39}Ar geochronometer are due to the refinement of the decay constants [*Renne et al.*, 2010, 2011] and the improved mass-spectrometric instrumentation [e.g., *Phillips and Matchan*, 2013].

Neutron fluences (ϕ; i.e., time integrated neutron fluxes, φ) in nuclear reactors are not homogeneous [e.g., *Dalrymple et al.*, 1981; *Renne et al.*, 2009]. Therefore, samples and geological age standards receive different neutron fluences. For irradiation facilities without sample rotation, this is accounted for by a three-dimensional distribution of the geological age standards and interpolation of determined J-values [e.g., *Morgan et al.*, 2013]. For rotating irradiation facilities, it is assumed that the rotation eliminates radial neutron

fluence gradients (e.g., McMaster reactor [*Clark et al.*, 1998]; FRG1 reactor [*Schwarz and Trieloff*, 2007]; 49-2 reactor [*Wang et al.*, 2009]), while *Foland et al.* [1989] briefly documented a radial fluence gradient at the Ford Nuclear Reactor, despite sample rotation and attributed it to uneven rotation of the container.

We observed radial neutron fluence gradients in irradiations in the rotating channels of two reactors and concluded that the assumption that sample rotation eliminates residual radial gradients should be tested for each reactor and irradiation. In this study, we concentrate on LVR-15 while results from FRG1 that was closed in 2010 are used for comparison. We monitored the fast-neutron fluence distribution with the ^{58}Ni(n$_f$,p)^{58}Co reaction and spectrometric measurements of the γ-activities associated with the subsequent radioactive decay of ^{58}Co. This approach was described in *Dalrymple et al.* [1981], but seems to be reported only (with Fe wire) from the BR-2 reactor in Belgium [e.g., *Boven et al.*, 2001; *Ivanov et al.*, 2003]. We extended the determination of relative variation of neutron fluences by *Dalrymple et al.* [1981] to the calculation of absolute neutron fluences based on the equations of *Martin and Clare* [1963]. In order to explain radial neutron fluence gradients despite rotation, we discuss reactor-specific differences in the neutron flux field, shielding effects, and geometric effects of loading and unloading, possible tilt and shift of the sample container during irradiation and compare our results with a 3-D model of the fast-neutron flux distribution in the reactor core of LVR-15.

2. Methods

2.1. Metallic Neutron Fluence Monitors

Figure 1 compares the cross-section σ(E >1 MeV) of the ^{39}K(n$_f$,p)^{39}Ar reaction with that of other nuclear reactions used for measuring the fast-neutron fluences in nuclear reactors. The relative abundance of neutrons in the ^{235}U-fission neutron flux spectrum makes the 1–5 MeV range the most relevant for ^{39}K activation [*Renne et al.*, 2005]. The σ(E) of ^{32}S(n$_f$,p)^{32}P, ^{54}Fe(n$_f$,p)^{54}Mn, and ^{58}Ni(n$_f$,p)^{58}Co are similar to that of

φ(E) calculated neutron-flux spectra in LVR-15:

--- FGA012
--- FGA014
--- φ(E) ^{235}U fission neutron flux spectrum [*Watt*, 1952]

σ(E) cross-sections:

— ^{39}K(n,p)^{39}Ar		— ^{46}Ti(n,p)^{46}Sc
— ^{58}Ni(n,p)^{58}Co		— ^{47}Ti(n,np)^{46}Sc
— ^{27}Al(n,a)^{24}Na		— ^{54}Fe(n,p)^{54}Mn
— ^{32}S(n,p)^{32}P		— ^{63}Cu(n,a)^{60}Co

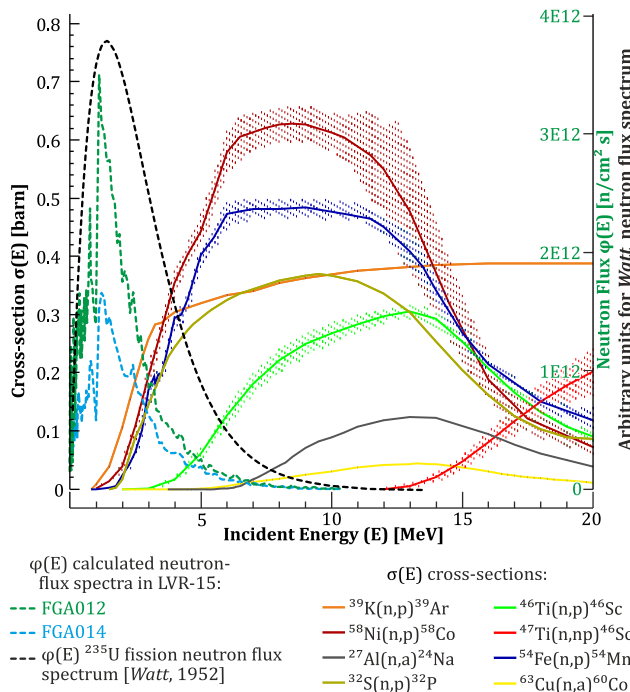**Figure 1.** Cross sections, σ(E) (left scale), and range of experimental data, where available, of the ^{39}K(n$_f$,p)^{39}Ar reaction and other reactions used for monitoring fast-neutron fluences, as a function of the neutron energy (plotted with IAEA software ZVView 9.2) [*Chadwick et al.*, 2011]. A ^{235}U fission neutron flux spectrum (stippled line) [*Watt*, 1952] and neutron flux spectra of irradiations FGA012 and FGA014 in LVR-15, calculated by MCNPX software 2.7.0 [*Pelowitz*, 2011] with ENDF/B-VII.1 data libraries (in SAND-II 640 neutron energy group interpretation of neutron flux) [*Chadwick et al.*, 2011] represent the energies of neutrons available for the activation reactions (right scale).

^{39}K(n$_f$,p)^{39}Ar. However, S has a low melting point and is chemically reactive. The advantages of ^{58}Ni(n$_f$,p)^{58}Co [e.g., *Dalrymple et al.*, 1981] over ^{54}Fe(n$_f$,p)^{54}Mn [e.g., *Boven et al.*, 2001] are the noncorroding properties of Ni and a σ(E) closer to that of ^{39}K(n$_f$,p)^{39}Ar for the relevant neutron energy spectrum. The main disadvantage is the thermal-neutron burn up of $^{58(m)}$Co, which must be corrected for if no thermal-neutron shielding (Cd cover) is applied (supporting information) [*Hogg et al.*, 1962; *Martin and Clare*, 1963]. Cd covering reduces thermal-neutron burn up of $^{58(m)}$Co, but has no effect on the fast-neutron spectrum because the Cd cutoff energy for neutron absorption is approximately 0.5 eV.

We included Ni fast-neutron fluence monitors (4 mm diameter foils of 0.01 mm thickness weighing ~1.1 mg) in contact with geological age standards and geochronological samples in irradiation FGA002 in the FRG1

reactor (Geesthacht, Germany) and in irradiations FGA012 and FGA014 in the LVR-15 reactor (Husinec—Řež, Czech Republic). To avoid problems from material loss potentially caused by neutron radiation embrittlement, the Ni-foil was sandwiched into Al-foil and die-cut. The $^{58}Ni(n_f,p)^{58}Co$ reaction rates (supporting information), and thus intensity of the 811 keV γ-peaks associated with $^{58}Co \rightarrow ^{58}Fe$ decay [*Andersson et al.*, 1986], are proportional to the fast-neutron fluences ϕ_f. In FRG1, we used Cd shielding to minimize thermal-neutron burn up of $^{58(m)}Co$ [*Hogg et al.*, 1962]. In LVR-15, we included Al-1%Co (IRMM 528RA; 8 mm diameter foils of 0.1 mm thickness weighing $\sim$14 mg) thermal-neutron fluence monitors and measured the 1332.5 keV γ-peaks associated with the $^{60(m)}Co \rightarrow ^{60}Ni$ decay following the $^{59}Co(n_{th},\gamma)^{60(m)}Co$ activation reaction [*Andersson et al.*, 1986] to calculate the thermal-neutron fluences ϕ_{th} (supporting information, Formula 1). The results were used to calculate the fast-neutron fluences ϕ_f based on *Martin and Clare* [1963, equation (5)] (supporting information, Formula 2). This equation takes into account the production of isomeric and ground-state ^{58}Co, the activation of both states to ^{59}Co, as well as their decay to ^{58}Fe during and subsequent to the irradiation; we implemented a correction for decay during measurement.

2.2. Gamma-Spectrometry
The γ-activities were measured on an EG&G Ortec 38% HPGe(Li) detector at 10 cm (Ni-foils) and 20 cm (Co-foils) nominal sample-detector separation similar to the setup of *Curvo et al.* [2013]. The foils from each irradiation were measured in a continuous measurement series within a period of less than 15 days, two per day. Peak evaluation was carried out using the GammaVision software Version 5.10. The integration intervals were fixed and centered on the channel with the maximum counts, whose position shifted by less than 1 keV within each measurement series. The detector resolution varied somewhat between the measurement series with the full peak width at half maximum around 2 keV. The detection efficiencies (ε_p) and measurement geometries were recalibrated for each measurement series using the FZ203 multipeak ^{152}Eu standard (43.6 kBq $\pm$ 3% at 2σ; $T_{1/2}$ = 4943 days; certified by AEA Technology QSA GmbH, 38110 Braunschweig, Germany; calibration date 9 December 1999). The relative counting uncertainty of the calibration measurements—that is important for comparison of results from different irradiations as in Figure 2—is $<$0.3% (precision). The quoted absolute uncertainty of 3% is the external uncertainty of the standard (accuracy).

2.3. Uncertainty Calculation
To determine relative ϕ_f variations, only sources of relative uncertainty must be considered. The measurement order of the foils was randomized to rule out any effect of instrumental drift.

The remaining sources of uncertainty are (1) the statistical weighing uncertainty, (2) the statistical counting uncertainty, and (3) a random uncertainty due to off-axis positioning of the foil above the detector. The 1σ standard uncertainty (reproducibility) of the Mettler Toledo XP6 Microscale used for weighing is $<$0.0008 mg, equivalent to a (conservative) relative 1σ weighing uncertainty of 0.07% for the Ni-foils. The statistical uncertainty of the gamma activities is calculated by the GammaVision software, assuming a Poisson distributed counting uncertainty and a minor term accounting for the uncertainty of the background correction. At least 1,000,000 counts were collected to attain relative 1σ counting uncertainties $<$0.1%. Typical counting uncertainties are between 0.06 and 0.08%. Off-axis sample positioning was observed to have an effect of 1.4% for a deliberate horizontal displacement of 13.5 mm. We estimate the maximum unintentional positioning error to be $<$0.6 mm and assume a relative 1σ uncertainty of 0.03%. The weighing, counting, and positioning uncertainties were propagated through formula 5 of *Martin and Clare* [1963] using a Monte Carlo method. Each variable was sampled from a Gaussian distribution, with its measured value as mean and its estimated uncertainty as standard deviation. The resulting fluence distributions are symmetric with relative standard deviations between 0.13% and 0.21%, averaging 0.17%.

2.4. Irradiation Procedure
The samples and foils are mounted in drill holes in high-purity Al-disks that are stacked to form the irradiation container (photograph in supporting information). The discussed irradiations contained mineral separates of mica, K-feldspar, and hornblende ($\leq$150 mg, mostly $\sim$10 mg per sample hole). In LVR-15, the container is enclosed by a waterproof Al-capsule that is weighted with lead to make it sink in the reactor. A taper at the lower part of the Al capsule is necessary to adjust the lid and prevent it from sliding into the capsule. This makes a larger diameter necessary allowing the sample container to shift by 3 mm from the center and tilt inside the Al-capsule (Figure 4a). The maximum total tilt depends on the height of the

container and amounts to 7.6° for the highest (60 mm, FGA012) and 14.6° for the shortest (30 mm, FGA014). The Al-capsule can shift by 1.9 mm from the center of the irradiation channel (Figure 4a) and tilt up to 1.7°.

The sample containers are loaded and unloaded by a semiautomatic grab system. During loading and unloading, the sample container is not rotating. The operation takes about 90 s each way, 30 s of which are spent within the core of the reactor. The best vertical position of the irradiation container is aimed to be at the middle of the fuel assemblies, which is realized by filling the rotating channel with dummy capsules. For some irradiations, the reactor was started after loading and/or stopped before unloading of the samples as specified in Table 1. The geometries and procedures in FRG1 are similar.

2.5. Analysis of Geological Age Standards

Fish Canyon Tuff sanidine (FCT) [*Cebula et al.*, 1986; *Renne et al.*, 1998] geological age standard was included in irradiations FGA002, FGA003, FGA012, FGA014, and FGA016 and a laboratory internal muscovite standard MK290 (calibrated against FCT) in FGA015 to determine the J-values. In FGA003, FGA015, and FGA016, the geological age standards were radially distributed in the irradiation container permitting an estimate of the radial fluence gradient in these irradiations (Table 1). All samples were analyzed with a GV Instruments ARGUS multicollector noble gas mass spectrometer. Detailed analytical procedures are described in *Pfänder et al.* [2014].

3. Results

3.1. Comparison of J-Values and Neutron Fluences

Figure 2 shows the fast-neutron fluences (ϕ_f) determined with Ni-foils plotted against J-values determined with geological age standards placed in direct contact with the Ni-foils. All three data sets show clear linear correlations: FGA012 and FGA014 in LVR-15 define indistinguishable trends with correlation coefficients (R) for regression lines through the origin of 0.89 and 0.99. Their slopes are ~4% lower than that of FGA002 from FRG1 and ~20% lower than the theoretical estimate calculated from isotopic data and spectrum-averaged cross sections (Figure 2; supporting information).
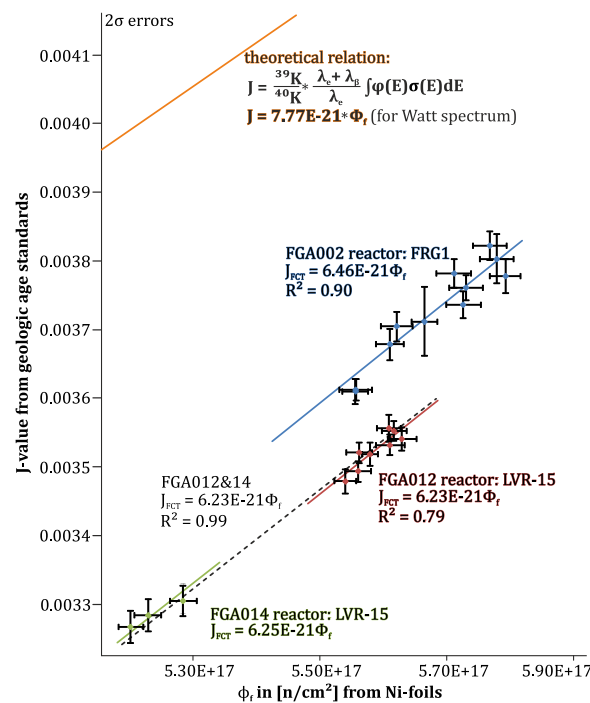
3.2. ϕ_f-Fluence Gradients

We calculated the fluence gradients from the ϕ_f (Ni-foils) and J-values (geological age standards) at known positions in the irradiation container. In all cases, a gradient in an acute angle to the axis of the container is observed (Figure 3). We computed the radial gradients ($\nabla_r\phi_f$) from the maximum difference within each irradiation disc and the axial gradients ($\nabla_a\phi_f$) from subjacent positions in the stack. The $\nabla_r\phi_f$ are based on four or more data points per disk; where fewer are available (FGA002 and FGA003), the listed $\nabla_r\phi_f$ are minimum estimates. Table 1 summarizes the results for the six irradiations in FRG1 and LVR-15, at different reactor powers and for different irradiation times. Figure 3 shows the variation of ϕ_f for FGA002, FGA012, FGA014, and J-values for FGA015 approximating a gradient along a space diagonal.

Figure 2. Correlation between fast-neutron fluences (ϕ_f) determined with Ni-foils and J-values determined from Co-irradiated geological age standards. The equations describe the fitted regression lines through the origin and the theoretical relation calculated with spectrum-averaged cross sections and R^2 correlation coefficients.

Table 1. Irradiation Details With Disks and Subjacent Holes Indicated for Each Computed Gradient

Irradiation	Reactor	Duration (s)	End Date, Time	Radial Gradients $\nabla_r\phi_f$ (%/cm)	Axial Gradient $\nabla_a\phi_f$ (%/cm)	Specifications
FGA002	FRG1	604800	13 Jun 2008, 13:39	>0.02 (D1) >0.5 (D2) >0.3 (D3) >1.8 (D4) >0.3 (D5)	1.5 (H10) 2.2 (H11) 1.9 (H12)	10 s per rotation; Cd-shielding; 5 MW; gradients from Ni-foils; only 2–3 points per disk give minimum radial gradients
FGA003	FRG1	432000	24 Aug 2008, 13:47	>0.5 (D1) >1.4 (D2) >0.6 (D3) >1.7 (D4) >0.3 (D5)	0.1 (H10) 1.7 (H12) 5.9 (H14) 4.3 (H18)	10 s per rotation; Cd-shielding; 5 MW; gradients from geological age standards; only two points per disk give minimum radial gradients
FGA012	LVR-15	9000	30 Oct 2012, 18:24	1.9 (D1) 1.2 (D4) 0.9 (D7) Mean: 1.3	0.4 (H1) 0.6(H3) 0.2 (H5) 0.5 (H11) Mean: 0.41	10 s per rotation; ∼10 MW; gradients from Ni-foils
FGA014	LVR-15	14400	31 Jul. 2013, 15:39	1.8 (D1) 1.9 (D2) 2.2 (D3) Mean: 2.0	1.0 (H3) 0.9 (H6) 1.4 (H9) 1.4 (H11) Mean: 1.2	10 s per rotation; ∼5 MW; gradients from Ni-foils
FGA015	LVR-15	57600	3 Dec 2013, 09:00	0.2 (D1) 0.2 (D2) 0.5 (D3) 0.4 (D4) 0.5 (D5) Mean: 0.4	0.8 (H1) 0.4 (H4) 0.4 (H7) 0.5 (H10) Mean: 0.5	10 s per rotation; ∼8 MW; gradients from Ni-foils; reactor stopped at loading and unloading
FGA016	LVR-15	6600	3 Dec 2013, 09:00	0.9 (D1) 0.6 (D3) Mean: 0.7	2.1 (H1) 1.5 (H3) 2.1 (H5) 1.8 (H7) 1.5 (H9) Mean: 1.8	10 s per rotation; ∼8 MW: gradients from geological age standards Dropped on top of FGA015; reactor stopped at unloading

3.2.1. Axial Fluence Gradients ($\nabla_a\phi_f$)

The maximum $\nabla_a\phi_f$ is 5.9 %/cm for FRG1 and 2.1 %/cm for LVR-15 (Table 1). In FRG1, the variation of $\nabla_a\phi_f$ ranges from 0.2 to 5.9 %/cm, while it is more uniform in LVR-15, ranging from 0.3 to 0.5 %/cm per irradiation. The fast-neutron fluence increases toward the top (FGA002, FGA003, FGA015) or bottom of the container (FGA012, FGA014, FGA016). FGA016 was piled on top of FGA015 for the last part of the irradiation cycle. ϕ_f increases upward in FGA015 and downward in FGA016. No correlation between irradiation time, reactor power, and magnitude of $\nabla_a\phi_f$ is observed.

3.2.2. Radial Fluence Gradients ($\nabla_r\phi_f$)

The maximum $\nabla_r\phi_f$ are 1.8 %/cm in FRG1 and 2.2 %/cm in LVR-15 (Table 1). The irradiation averages range from 0.4 to 1.1 %/cm. The minimum estimates of $\nabla_r\phi_f$ for irradiations FGA002, and FGA003 in FRG1 exhibit a large scatter owing to poorer statistics. In LVR-15, $\nabla_r\phi_f$ varies <0.4 %/cm between the sample discs within one irradiation can except for irradiation FGA012 where the variation reaches 1 %/cm. The radial gradients systematically decrease upward or downward for the irradiations in LVR-15. No relation with irradiation time, reactor power and magnitude of $\nabla_r\phi_f$ is observed.

For comparison, the reported $\nabla_r\phi_f$ in nonrotating irradiation facilities of several reactors used for ^{40}Ar/^{39}Ar sample irradiation are: 0.5 %/cm in the GSTR (Denver, USA) [*Dalrymple et al*., 1981], <0.1–0.85 %/cm in the OSTR (CLICIT channel; Corvallis, USA) [*Jourdan and Renne*, 2014; *Renne et al*., 1998], 13 %/cm in the JMTR (Oarai, Japan) [*Ishizuka*, 1998], ∼13 %/cm in the HIFAR (Sydney, Australia) [*Glasstone and Edlund*, 1952], and ∼2 %/cm in the 49-2 reactor (Beijing, China) [*He et al*., 2006]. For rotating facilities, the $\nabla_r\phi_f$ are ≤4% on one "plate" (no diameter given) in the Ford Nuclear Reactor (Ann Arbor, USA, now closed) [*Foland et al*., 1989] and ≤0.24 %/cm in the GSTR (Denver, USA; T. DeBey, personal communication, 2014).
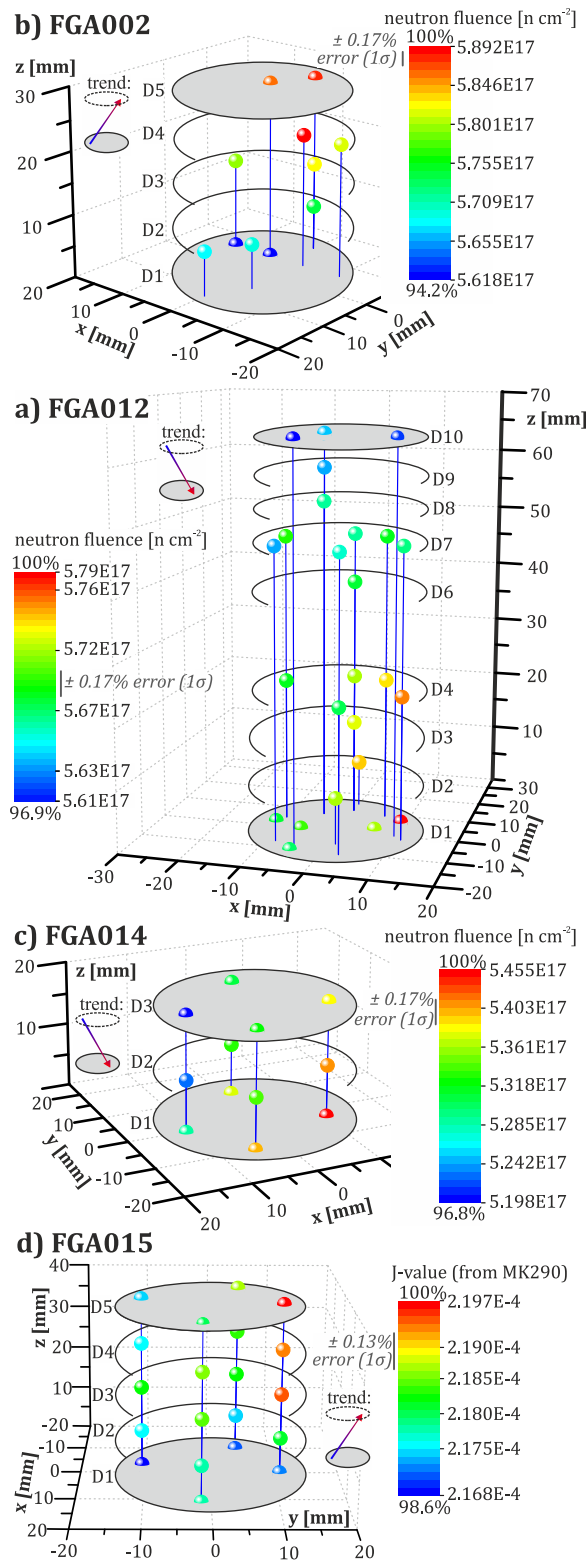
Figure 3. Scaled 3-D plots of fast-neutron fluences determined with Ni-foils for (a) FGA012 (LVR-15), (b) FGA002 (FRG1), (c) FGA014 (LVR-15), and (d) J-values from geological age standards for FGA015 (LVR-15). Mean uncertainties are indicated along the color code. Axial direction is parallel z.

3.3. NODER Fast-Neutron Flux Models

We modeled the 3-D distribution of the fast-neutron flux (φ_f; 0.821–10 MeV neutrons) across the core of the LVR-15 reactor, with emphasis on the irradiation channel, and extracted a vertical and two perpendicular horizontal cuts for the geometry of FGA012 (Figure 4). The NODER code [*Ernest*, 2006] used for this calculation is a diffusion operational code developed for the LVR-15 reactor for determining the fission density and neutron flux distribution across the core. The model accounts for the whole core, consisting of fuel assemblies, control rods, beryllium assemblies and aluminum irradiation channels that are homogenized within a fine rectangular grid for calculation. The model takes fuel burn up and regulation during the operational cycle into account. The schematic core setup of LVR-15 during irradiation FGA012 is given in the supporting information.

Figure 4b shows the vertical distribution of φ_f along the active height (60 cm containing uranium) of the fuel assembly. It can be approximated by a sinusoidal function with 65% variation between center and tips. The neutron flux vertical maximum might deviate by up to 5 cm from the geometrical center of the reactor core, caused by asymmetries in reactor core loading and regulation pattern (M. Koleška et al., Capabilities of the LVR-15 research reactor for production of medical and industrial radioisotopes, submitted to *Journal of Radioanalytical and Nuclear Chemistry*, 2014). In the horizontal (radial) direction, the fast-neutron flux field is a complex superposition of inverse-square functions, describing the decrease of φ_f with distance from each fuel assembly, and exponential decay functions describing neutron shielding and slowing down in the moderator (water, beryllium). Within the

irradiation channel, the spread of φ_f values is 17%, while the gradients are between -5.57 and 7.17 %/cm indicating a strongly nonlinear flux field for the investigated area.

4. Discussion

Axial fluence gradients across irradiation containers are well known and routinely corrected for in $^{40}Ar/^{39}Ar$ dating [*McDougall and Harrison*, 1999]. In contrast, radial fluence gradients are usually assumed to be eliminated in rotating irradiation channels. According to our observations, however, radial gradients of the order of 1–2 %/cm can occur despite rotation, potentially introducing significant uncertainties to $^{40}Ar/^{39}Ar$ dates.

4.1. Reactor-Specific Differences in Neutron Flux Field and Gradients

The empirical correlations between ϕ_f and J-value are strong (Figure 2), but the fitted slopes deviate from the theoretical estimate. This is the result of using spectrum-averaged cross sections for calculating ϕ_f. These assume a *Watt* [1952] U^{235}-fission neutron flux spectrum that only approximates the true $\phi(E)$ distribution (stippled functions in Figure 1). A probably minor contributor to the deviation is the uncertainty of the experimentally determined $\sigma(E)$ cross-section functions. To calculate J-values from Ni-foils, the $\sigma(E)$ functions of the $^{58}Ni(n_f,p)^{58}Co$ and $^{39}K(n_f,p)^{39}Ar$ reactions must be convoluted with the true $\phi(E)$, which, however, is not exactly determined. The difference between the indistinguishable correlations for the irradiations in LVR-15 and that in FRG1 is the result of different $\phi(E)$ in these reactors, caused by different fuel, reactor design and irradiation positions.

The variation of axial gradients between individual irradiations in the same reactor is explained by a varying axial position in the core and the fuel cycle. The exceptional variation and high maximum of $\nabla_a\phi_f$ for irradiation FGA003 in FRG1, compared to $\nabla_a\phi_f$ of FGA002 in the same reactor (Table 1), can be the result of
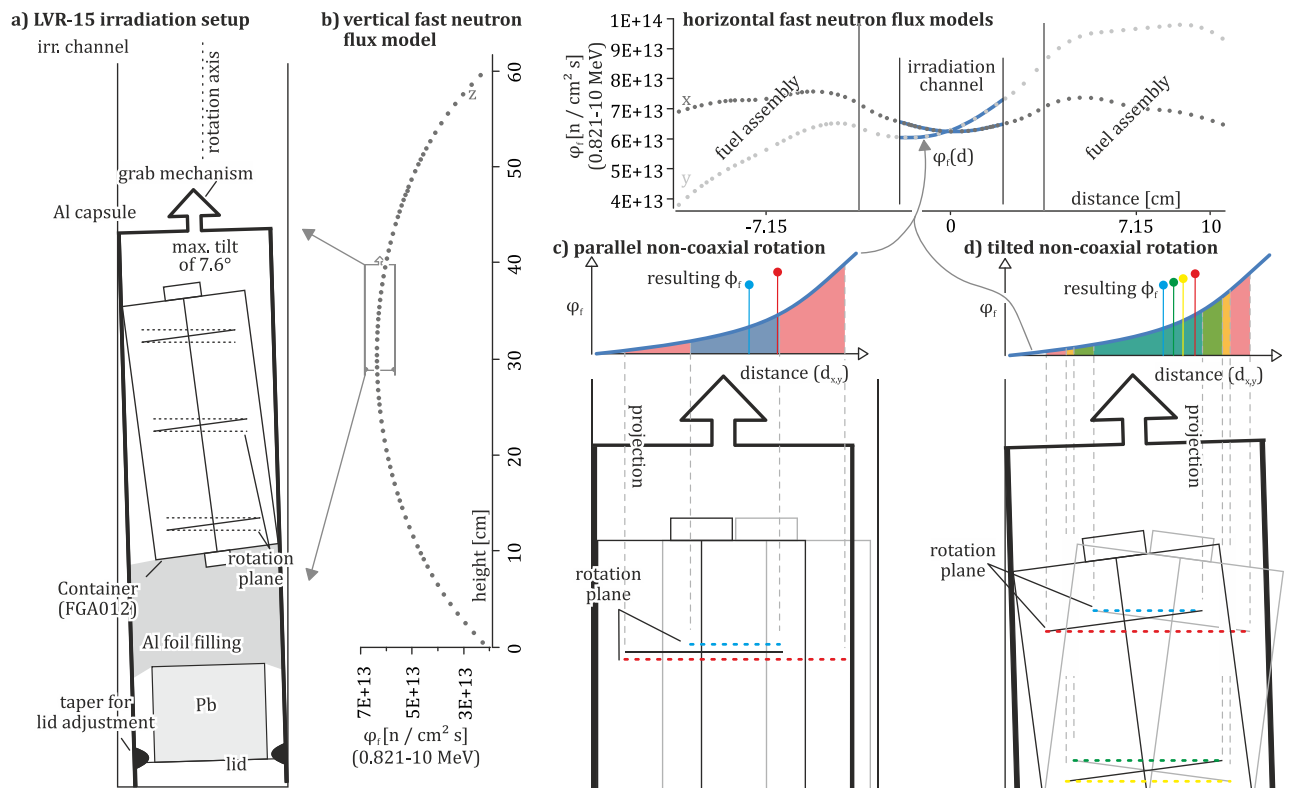

Figure 4. Scaled irradiation setup of reactor LVR-15 and neutron flux models. (a) Tilting of the container produces apparent radial gradients that are a fraction of the axial gradient. (b) NODER model [*Ernest*, 2006] of the fast-neutron flux along a vertical and two perpendicular horizontal sections through the LVR-15 reactor core for the geometry of FGA012 highlighting the nonlinear fast-neutron flux within the irradiation channel. (c) Rotation planes of two sample positions (blue and red) in an off-center container in the irradiation channel. The resulting ϕ_f is the integral over the irradiation time ($\varphi_f[x(t),y(t),z(t)]dt$; t = time during irradiation), which is different for the blue and red sample. (d) Detail of (Figure 4a) comprising tilting and non-coaxial rotation resulting in along-axis variation of radial fluence gradients.

suboptimal positioning, a factor that is to some extent within the control of the operator and is not necessarily representative of the reactor. In the piled irradiation of FGA015 and FGA016, one container was below and the other above the midpoint. The $\nabla_a\phi_f$ in LVR-15 are, in general, somewhat smaller than in FRG1, although the values for those for FGA016 are significantly higher than those for FGA012, FGA014, and FGA015 in the same reactor.

4.2. Shielding Effects
Except for the sample material and the weighing lead the irradiation can consists of high-purity Al and ambient air that can be regarded as fast-neutron transparent. As shown by *Tetley* [1978] and *Dalrymple et al.* [1981], shielding effects of the irradiated amounts of sample material are small and expected to be below our resolution. Furthermore, shielding by samples cannot explain the observed systematic gradients over the entire sample container (Figure 3), but would rather cause shorter wavelength fluctuations.

With a MCNPX (Monte Carlo N-Particle eXtended) calculation [*Pelowitz*, 2011], we modeled the influence of the 145 g of lead positioned 45 mm below the container for the irradiation geometry of FGA012 in LVR-15. For the lowermost disk, the <0.1 MeV neutron flux decreases by about 1% with the lead present, but no influence on the fast neutrons is observed. We do not consider shielding effects to be of importance for the observed gradients.

4.3. Sample Handling
During loading and unloading, the lower end of the container enters the core first and leaves it last, which results in an estimated residual axial fluence gradient of 0.1 %/cm for a 60 min irradiation. The upward and downward increasing ϕ_f indicate that this effect is eclipsed by that of the vertical position relative to the ϕ_f maximum. Because the irradiation times are multiples of the irradiation channel's revolution period (10 s), the orientation of the container is the same during loading and unloading and a residual radial flux gradient could add up. However, there is no distinct correlation between $\nabla_r\phi_f$ and the fraction of handling time to total irradiation time (Table 1; supporting information). Unrealistic horizontal flux gradients of 50–400 %/cm would be required to account for the observed residual radial gradients. Moreover, radial gradients are also observed in FGA015 which was loaded and unloaded during reactor shutdown.

The irradiation times in the FRG1 reactor are much longer than in LVR-15. Handling time is thus much shorter compared to the total irradiation time. Nevertheless, similar radial fluence gradients were observed as in the LVR-15 reactor.

4.4. Tilt and Shift of the Irradiation Container and Asymmetric Rotation
Figure 4a shows how tilt of the container creates apparent $\nabla_r\phi_f$ that amount to 13.1% (FGA012) to 25.1% (FGA014) of $\nabla_a\phi_f$ depending on the maximum angle discussed in section 2.4. The observed $\nabla_r\phi_f$ are, however, of the same order as the $\nabla_a\phi_f$. Still, this mechanism can contribute to the observed radial gradients. The possible shifting of the container in the irradiation channel (Figure 4c) by up to 5 mm, combined or not with tilting (Figures 4c and 4d), leads to noncoaxial rotation. Figures 4c and 4d show the paths of exemplary samples (red, blue, green, yellow) and their projections on the function $\varphi_f(d)$ (d, distance). For nonlinear $\varphi_f(d)$, the resulting ϕ_f of the samples will differ and build a residual $\nabla_r\phi_f$. The apparent systematic along-axis variation of observed $\nabla_r\phi_f$ (Table 1) supports a case as in Figure 4d. This effect can be eliminated by precise coaxial rotation of the container. Even with coaxial rotation, a nonlinear flux $\varphi_f(d)$ creates residual $\nabla_r\phi_f$ between samples at positions on the sample discs following circular paths with a different radius (Figure 4c). Therefore, such configurations should be avoided, or separate J-values need to be determined for each radius.

4.5. Potential of Metallic Fluence Dosimetry
The reached average precision of 0.17% (1σ) for ϕ_f with Ni-foil is similar to routinely achieved J-value precisions based on geological age standards in many labs, while first studies with the newest generation of noble gas mass spectrometers report significantly higher precisions (0.013%, 1σ) [*Phillips and Matchan*, 2013]. All discussed sources of uncertainty (section 2.3) can be reduced to reach higher precisions by, e.g., increasing the weight of the foil (doubling would decrease the counting and weighing uncertainty by ~30% and 50%, respectively) or using a better scale. The geometry of the γ-spectrometer can be optimized to rule out off-axis positioning and decrease nominal sample-detector separation in order to reach higher counting efficiencies. Ultimately the Poisson distributed counting uncertainty impedes improvements, but precisions of ~0.05% seem well within reach.

Conditional on a precise knowledge of the fast-neutron fluence distribution ϕ_f(E) in the irradiation channel and of the (relative) cross-sections σ_f(E) of the ^{39}K(n$_f$,p)^{39}Ar and ^{58}Ni(n$_f$,p)^{58}Co reactions, γ-spectrometry of Ni-foils could be used to calculate J-values that are independent of the ages of geological standards. Provisional estimates based on spectrum-averaged fluences and cross sections are ~16% (FRG1) to ~20% (LVR-15) too low. If this discrepancy could be eliminated by further research or by avoiding the spectral character of irradiation in a research reactor (e.g., by monoenergetic irradiation) [*Renne et al.*, 2005], metallic fluence dosimeters could be an alternative to geological age standards.

5. Conclusions

Ni-foils are useful to monitor the spatial variation of the fast-neutron fluence of sample irradiations for ^{40}Ar/^{39}Ar dating. In an extreme case, this technique allows one to include just one geological age standard per irradiation, tracking relative ϕ_f-variations with the Ni-foils. The advantages of using Ni-foils are their simple and cost-effective γ-spectrometric analysis, small dimensions and computable, negligible shielding of fast neutrons. Our measurements have an average precision of 0.17%, similar to routine J-value determinations based on geological age standards. Higher precisions could be reached with improvements to the technique such as more precise weighing or an improved geometry of the γ-spectrometry.

Despite rotation during irradiation, radial neutron fluence gradients of up to 1.8 %/cm (FRG1) and 2.2 %/cm (LVR-15), i.e., of the same magnitude as the axial gradients, are observed in six irradiations in two different reactors. Tilting of the container and irradiation capsule and noncoaxial rotation in a nonlinear fast-neutron flux field are the main factors responsible for these gradients. These effects can be suspended by precise coaxial rotation with a single radius. Loading and unloading of the samples with interrupted rotation are only minor contributors to radial fluence gradients. We conclude that for containers with radial extent in not entirely coaxial setups, radial fluence monitoring is essential for high-precision ^{40}Ar/^{39}Ar dating, even in fast rotating irradiation facilities.

References

Andersson, P., L. P. Ekström, and J. Lyttkens (1986), Nuclear data sheets for A = 60, *Nucl. Data Sheets*, 48, 251–344.

Baksi, A. K., D. A. Archibald, and E. Farrar (1995), Intercalibration of 40Ar/39Ar dating standards, *Chem. Geol.*, 129, 307–324.

Boehnke, P., and T. M. Harrison (2014), A meta-analysis of geochronologically relevant half-lives: What's the best decay constant?, *Int. Geol. Rev.*, 56(7), 905–914, doi:10.1080/00206814.2014.908420.

Boven, A., P. Pasteels, S. P. Kelley, L. Punzalan, B. Bingen, and D. Demaiffe (2001), ^{40}Ar/^{39}Ar study of plagioclases from the Rogaland anorthosite complex (SW Norway); an attempt to understand argon ages in plutonic plagioclase, *Chem. Geol.*, 176, 105–135.

Cebula, G. T., M. J. Kunk, H. H. Mehnert, C. W. Naeser, J. D. Obradovich, and J. F. Sutter (1986), The Fish Canyon tuff, a potential standard for the 40Ar/39Ar and fission-track methods, *Terra Cognita*, 6, 139–140.

Chadwick, M. B., et al. (2011), ENDF/B-VII.1: Nuclear Data for Science and Technology: Cross-sections, covariances, fission product yields and decay data, *Nucl. Data Sheets*, 112, 2887–2996.

Clark, A. H., D. A. Archibald, A. W. Lee, E. Farra, and C. J. Hodgson (1998), Laser probe ^{40}Ar/^{39}Ar ages of early- and late-stage alteration assemblages, Rosario porphyry copper-molybdenum deposit, Collahuasi district, I region, Chile, *Econ. Geol.*, 93, 326–337.

Curvo, E. A. C., R. Jonckheere, S. Guedes, P. J. Iunes, J. C. Hadler, S. Unterricker, and L. Ratschbacher (2013), A comparison between neutron-fluence measurements using metal-activation monitors and standard glasses calibrated via thin uranium-fission monitors and via ηq method, *Radiat. Meas.*, 53–54, 38–44, doi:10.1016/r.admeas.2013.03.002.

Dalrymple, G. B., E. C. Alexander Jr., M. A. Lanphere, and G. P. Kraker (1981), Irradiation of samples for ^{40}Ar/^{39}Ar dating using the Geological Survey TRIGA reactor, U.S. Geol. Surv. Prof. Pap. 1176.

Ernest, J. (2006), Abstrakt výpočtového programu NODER—Rev. 1, *Tech. Rep. ÚJV-12695R*, ÚJV Řež, Řež, Czech Republic.

Foland, K. A., J. F. Chen, J. S. Linder, C. M. B. Henderson, and I. M. Whillians (1989), High-resolution ^{40}Ar/^{39}Ar chronology of multiple intrusion igneous complexes, *Contrib. Mineral. Petrol.*, 102, 127–137.

Glasstone, S., and M. C. Edlund (1952), *The Elements of Nuclear Reactor Theory*, D. Van Nostrand, N. Y.

He, H. Y., X. L. Wang, F. Jin, Z. H. Zhou, F. Wang, L. K. Yang, X. Ding, A. Boven, and R. X. Zhu (2006), The ^{40}Ar/^{39}Ar dating of the early Jehol Biota from Fengning Hebei Province, northern China, *Geochem. Geophys. Geosyst.*, 7, Q04001, doi:10.1029/2005GC001083.

Hogg, C. H., L. D. Weber, and E. C. Yates (1962), *Thermal Neutron Cross Sections of the ^{58}Co Isomers and the Effect on Fast Fluence Measurements Using Nickel*, U.S. At. Energy Comm., Idaho Oper. Off., Idaho Falls, Idaho, USA.

Ishizuka, O. (1998), Vertical and horizontal distribution of the fast neutron flux in a single irradiation capsule and their significance in the laser-heating ^{40}Ar/^{39}Ar analysis: Case study for the hydraulic rabbit facility of the JMTR reactor, Japan, *Geochem. J.*, 32, 243–252.

Ivanov, A. V., A. A. Boven, S. B. Brandt, I. S. Brandt, and S. V. Rasskazov (2003), Achievements and limitations of the K-Ar and 40Ar/39Ar methods: What's in it for dating the Quaternary sedimentary deposits, *Berl. Paläobiol. Abh.*, 4, 65–75.

Jourdan, F., and P. R. Renne (2014), Neutron-induced ^{37}Ar recoil ejection in Ca-rich minerals and implications for ^{40}Ar/^{39}Ar dating, in *Advances in 40Ar/39Ar Dating: From Archaeology to Planetary Sciences*, Geol. Soc. Spec. Publ., 378, 33–52, doi:10.1144/SP378.15.

Kuiper, K. F., A. Deino, F. J. Hilgen, W. Krijgsman, P. R. Renne, and J. R. Wijbrans (2008), Synchronizing rock clocks of earth history, *Science*, 320, 500–504, doi:10.1126/science.1154339.

Martin, W. H., and D. M. Clare (1963), Determination of fast-neutron dose by nickel activation, *Nucl. Sci. Eng.*, 18, 468–473.

McDougall, I., and T. M. Harrison (1999), *Geochronology and Thermochronology by the $^{40}Ar/^{39}Ar$ Method*, 269 pp., Oxford Univ. Press, Oxford, U. K.

Morgan, L. E., D. F. Mark, J. Imlach, D. Barford, and R. Dymock (2013), FCs-EK: A new sampling of the Fish Canyon Tuff $^{40}Ar/^{39}Ar$ neutron flux monitor, in *Advances in $^{40}Ar/^{39}Ar$ Dating: From Archaeology to Planetary Sciences*, edited by F. Jourdan, D. F. Mark, and C. Verati, pp. 63–67, vol. 378, *Geol. Soc. Spec. Publ.*, London, U. K., doi:10.1144/SP378.21.

Onstott, T. C., M. L. Miller, R. C. Ewing, G. W. Arnold, and D. S. Walsh (1995), Recoil refinements: Implications for the $^{40}Ar/^{39}Ar$ dating technique, *Geochim. Cosmochim. Acta*, 59, 1821–1834.

Pelowitz, D. B. (Ed.) (2011), *MCNPX User's Manual, Version 2.7.0—LA-CP-11–00438*, Los Alamos Natl. Lab., New Mexico, USA.

Pfänder, J. A., B. Sperner, L. Ratschbacher, A. Fischer, M. Meyer, M. Leistner, and H. Schaeben (2014), Highresolution $^{40}Ar/^{39}Ar$ dating using a mechanical sample transfer system combined with a hightemperature cell for step heating experiments and a multicollector ARGUS noble gas mass spectrometer, *Geochem. Geophys. Geosyst.*, 15, 2713–2726, doi:10.1002/2014GC005289.

Phillips, D., and E. L. Matchan (2013), Ultra-high precision $^{40}Ar/^{39}Ar$ ages for Fish Canyon tuff and Alder Creek Rhyolite sanidine: New dating standards required?, *Geochim. Cosmochim. Acta*, 121, 229–239.

Renne, P. R., C. C. Swisher, A. L. Deino, D. B. Karner, T. L. Owens, and D. J. DePaolo (1998), Intercalibration of standards, absolute ages and uncertainties in $^{40}Ar/^{39}Ar$ dating, *Chem. Geol.*, 145, 117–152.

Renne, P. R., K. B. Knight, S. Nomade, K. N. Leung, and T. P. Lou (2005), Application of deuteron-deuteron (d-d) fusion neutrons to $^{40}Ar/^{39}Ar$ geochronology, *Appl. Radiat. Isotopes*, 62, 25–32.

Renne, P. R., et al. (2009), Data reporting norms for $^{40}Ar/^{39}Ar$ geochronology, *Quat. Geochronol.*, 4, 346–352.

Renne, P. R., R. Mundil, G. Balco, K. Min, and K. R. Ludwig (2010), Joint determination of ^{40}K decay constants and $^{40}Ar*/^{40}K$ for the Fish Canyon sanidine standard, and improved accuracy for $^{40}Ar/^{39}Ar$ geochronology, *Geochim. Cosmochim. Acta*, 74, 5349–5367, doi:10.1016/j.gca.2010.06.017.

Renne, P. R., G. Balco, K. R. Ludwig, R. Mundil, and K. Min (2011), Response to the comment by W.H. Schwarz et al. on "Joint determination of ^{40}K decay constants and $^{40}Ar*/^{40}K$ for the Fish Canyon sanidine standard, and improved accuracy for $^{40}Ar/^{39}Ar$ geochronology" by P.R. Renne et al. (2010), *Geochim. Cosmochim. Acta*, 75, 5097–5100, doi:10.1016/j.gca.2011.06.021.

Roddick, J. C. (1983), High precision intercalibration of 40Ar-39Ar standards, *Geochim. Cosmochim. Acta*, 47, 887–898.

Schwarz, W. H., and M. Trieloff (2007), Intercalibration of ^{40}Ar-^{39}Ar age standards NL-25, HB3gr hornblende, GA1550, SB-3, HD-B1 biotite and BMus/2 muscovite, *Chem. Geol.*, 242, 218–231, doi:10.1016/j.chemgeo.2007.03.016.

Smith, P. W., N. M. Evensen, and D. York (1993), First successful ^{40}Ar-^{39}Ar dating of glauconies: Argon recoil in single grains of cryptocrystalline material, *Geology*, 21(1), 41–44.

Tetley, N. W. (1978), Geochronology by the 40Ar/39Ar technique using HIFAR reactor, PhD dissertation, Aust. Natl. Univ., Canberra.

Turner, G. (1995), Argon40-Argon39 dating: The optimization of irradiation parameters, *Earth Planet. Sci. Lett.*, 10, 227–234.

Wang, F., X. S. Zheng, J. I. K. Lee, W. H. Choe, N. Evans, and R. X. Zhu (2009), An $^{40}Ar/^{39}Ar$ geochronology on a mid-Eocene igneous event on the Barton and Weaver peninsulas: Implications for the dynamic setting of the Antarctic Peninsula, *Geochem. Geophys. Geosyst.*, 10, Q12006, doi:10.1029/2009GC002874.

Watt, B. E. (1952), Energy spectrum of neutrons from thermal fission of U^{235}, *Phys. Rev.*, 87, 1037–1041, doi:10.1103/PhysRev.87.1037.